Published in final edited form as:
Curr Pharm Biotechnol. 2014 ; 14(13): 1127–1133.

FRET Enhanced Fluorescent Nanodiamonds

Rafal Fudala[1], **Sangram Raut**[1], **Badri P. Maliwal**[1], **T. W. Zerda**[2], **Ignacy Gryczynski**[1,4], **Eric E Simanek**[3], **Julian Borejdo**[1,4], **Ryan Rich**[1,2], **Irina Akopova**, and **Zygmunt Gryczynski**[1,2,*]

[1]Center for Commercialization of Fluorescence Technologies, Department of Molecular Biology and Immunology, University of North Texas Health Science Center, 3500 Camp Bowie Blvd., Fort Worth, TX 76106, USA

[2]Department of Physics and Astronomy, Texas Christian University, TCU Box 298840, Fort Worth, TX 76129, USA

[3]Department of Chemistry, Texas Christian University, TCU Box 298840, Fort Worth, TX 76129, USA

[4]Department of Cell Biology and Genetics, University of North Texas Health Science Center, 3500 Camp Bowie Blvd, Fort Worth, TX 76106, USA

Abstract

Fluorescent nanodiamonds (FNDs) are one of the new and very promising biocompatible nanomaterials that can be used both as fluorescence imaging agent and a highly versatile platform for controlled functionalization to target and deliver a wide spectrum of therapeutic agents. Among the remarkable fluorescence properties are excellent photo-stability, emission between 600–700nm, quantum yield of 1 and moderately long fluorescence lifetimes. However the low absorption cross section of fluorescent $(N\text{-}V)^-$ centers limits FNDs' brightness. In this work we show that an approach based on the Forster resonance energy transfer (FRET) may significantly enhance the fluorescence signal observed from a single ND. We demonstrate that organic dyes (fluorophores) attached to the FND surface can efficiently transfer the excitation energy to $(N\text{-}V)^-$ centers. Multiple dyes positioned in close proximity to the ND facile surface may serve as harvesting antennas transferring excitation energy to the fluorescent centers. We propose that, with the help of some of the functional groups present on the FND surface, we can either directly link flurophores or use scalable dendrimer chemistry to position many organic dyes at a calibrated distance. Also, the remaining multiple functional groups will be still available for particle targeting and drug delivery. This opens a new way for designing a new type of theranostics particles of ultra-high brightness, high photostability, specific targeting, and high capacity for drug delivery.

Keywords

Fluorescence Nanodiamonds; Forester Resonance Energy Transfer (FRET); Fluorescence

*Address correspondence to this author at the Department of Physics and Astronomy, Texas Christian University, TCU Box 298840, Fort Worth, TX 76129, USA; Tel: 8172574209; Fax: 8172577742; zgryczynski@tcu.edu.

INTRODUCTION

Incorporating nanomaterials into biomedical imaging and diagnostics has emerged as a key area of research in the multi-disciplinary field of nanobiotechnology. The promise of nanomaterial-enabled drug delivery and diagnostics has great potential to revolutionize the fields of detection, diagnostics, and pharmacology, thereby helping to tackle diseases at a molecular level. In order to understand how complex biological systems function at the molecular level, it is essential that biomolecules and molecular processes be studied individually for a sufficiently long time and their interactions be directly imaged in vivo. These needs require imaging methods and imaging probes capable of reporting on molecular events and molecular interactions with high spatial and temporal resolution and accuracy.

As fluorescence is one of the most widely used tools in biomedical imaging and assays, the development of superior fluorophores and probes with specific properties is an active research area [1–6]. Among the many obstacles to successfully using a fluorescent probe to study biological systems, the most important are the relative level of background signal and probe photostability. An “ideal” probe will have a signal clearly different/stronger than that from sample autofluorescence (background), be photostable during the long imaging experiments, and not interfere with the target or surrounding. An even better, probe could also carry therapeutic agents. In other words it should be capable of becoming a part of multi-functional drug delivery nanoparticle.

Fluorescent nanodiamonds (FNDs) are one of the new classes of fluorescent probes with high potential to be very successful in practical imaging applications [7–17]. Fluorescent properties of FNDs are the result of point defects embedded in the crystal lattice. Among these impuriy centers are substitution nitrogen atoms next to vacancies (N-V). Nitrogen impurities may occur naturally in diamond crystals produced by the explosion technique. In natural or man-made diamond, nitrogen abundance is low, but it can be increased by implanting nitrogen ions. Vacancies can be generated by proton, electron, or heavy ion bombardment. Vacancies diffuse during the annealing process and combine with nitrogen to form neutral (NV) or negatively charged $(NV)^-$ fluorescing centers. The coexisting (N-V) and $(N\text{-}V)^-$ defect pairs result in broad absorption bands with the maximum around 560 nm, corresponding to the transition from a ground (^3A) state to an excited (^3E) state and emits fluorescence between 600 and 700 nm. FND probes have almost 100% quantum yield, relatively long fluorescence lifetimes (between 10 ns and 24 ns) and, importantly, do not photobleach even under intensive illumination [9, 12]. Fluorescent NDs may range in size from 4 – 100 nm and are biocompatible, nontoxic, chemically inert, and environmentally benign [9, 10]. Furthermore, the process of preparing FNDs also creates abundant carboxyl and hydroxyl or amino groups on the nanodiamond surface. These functional groups provide an easy route for labeling [11, 12] with the desired biomolecules for applications in targeted delivery and gene therapies. The critical limitation for fluorescence applications is the low absorption oscillator strength (extinction coefficient) of a single vacancy which results in a relatively low fluorescence brightness when compared to very high extinction coefficient organic probes. As an example, it will require tens of $(N\text{-}V)^-$ centers in a FND to have a brightness comparable to cyanine dyes or rhodamine B6 [18].

In this report we present a new approach based on the Forster resonance energy transfer (FRET) that has the potential to greatly enhance the absorption cross-section of ND particles to a level much higher than that of the best single organic dye. By introducing multiple organic dyes on the ND surface that are suitable energy donors to the $(N\text{-}V)^-$ color centers, we can achieve very large absorption cross-sections. Consequently, a radiationless energy transfer from the organic dye to the $(N\text{-}V)^-$ vacancy proves to be a very effective excitation of color centers. We use a simple physical attachment of bovine serum albumin (BSA) protein labeled with FITC molecules (~7 per BSA) to the ND surface. The results demonstrate effective distance dependent FRET from FITC to ND vacancies. This concept utilizes multiple organic dyes as “antennas” to absorb/harvest light and transfer excitation energy to the emissive center and is similar to chelated lanthanide probes where energy transfer from chelator excites the lanthanide atom [19]. Depending on the absorption spectrum of selected dyes, we can also tune the absorption of the probe to the desirable wavelength.

MATERIALS AND METHODS

Reagents and Materials

Bovine serum albumin-FITC conjugate was purchased from Sigma. The efficiency of FITC labeling was 7 FITC per BSA. FNDs were obtained from the Institute of Atomic and Molecular Sciences, Academia Sinica, Taiwan. Phosphate Buffer Saline (PBS) 10×, pH 7.4 was from MP Biomedicals and used as 1× dilution.

Conjugating BSA-FITC to FNDs

500 μg of fluorescent NDs were suspended in 500 uL of PBS, pH 7.4 and sonicated for 15 minutes. Separately, solution of FITC-BSA was prepared in PBS (pH 7.4). 50 μg of FITC-BSA was added to FND suspension and incubated overnight (12 hours) with gentle stirring. The suspension was centrifuged at 12,000 rpm to separate FND-protein complex and washed several times with PBS buffer and centrifuged again. Also suspension of FND-Protein complex was further dialyzed using a 100 kD dialysis bag for 6 hours against PBS buffer to remove any unbound BSA-FITC.

Sample Preparation

For all the measurements high dilutions of the original samples were used. A drop of FNDs or FND-Protein complex was placed on the special Menzel-Glaser microscopy glass slides and air dried for future measurements.

UV-Visible Absorption and Fluorescence Spectroscopy

UV-visible absorbance measurements were performed using a Cary 50 spectrometer (Varian Analytical Instruments, USA). Emission and excitation spectra in solution were measured using a Varian Cary Eclipse Fluorometer (Varian Analytical Instruments, USA). The measurements were made in 10 mm × 10 mm and 4 mm × 10 mm optical cuvettes for protein and diamonds respectively.

Confocal Microscopy

Measurements on a single molecule level were done with the custom equipped MicoTime 200 system from PicoQuant (Germany). The system is equipped with 4 detectors (two Perkin Elmer and two MPD) and 4 excitation laser diodes. For our measurements we used a 470 nm pulsed laser diode (20 MHz repetition rate) as excitation source and a Perkin Elmer detector. The microscope system worked with object piezo scanner configuration and OLYMPUS 60× water immerse objective NA 1.2. The excitation pulse width at the sample was below 100 ps. The time response of the Perkin Elmer detector has been estimated to be about 400 ps. For single molecule studies the FNDs or FND-Protein complexes were deposited on glass slides (Menzel-Glaser 20×20mm #1). With the confocal system, the wide field stage scanning reveals the positions of single spots. The laser beam could be then precisely positioned over the individual spots (FNDs or FND-Protein complexes) and fluorescence photons could be recorded simultaneously with respect to the very first pulse in the experiment and with respect to each individual pulse which initiated the photon (so called Time-Tagged Time Resolved (TTTR) mode [20]). For data analysis and interpretation the *SymPho Time v.4.3 software from PicoQuant was used. TCSPC histogramming for fluorescence lifetime fitting is readily possible from every recorded file and each selected part of the file (each selected segment of photon trace).

Data Analysis

The intensity decays were analyzed with a multi-exponential model using FluoFit v. 4 software (PicoQuant, GbmH.). The data for each experiment were fitted with the multi-exponential model:

$$I(t) = \sum_i \alpha_i \, exp(-t/\tau_i) \quad (1)$$

where τ_i are the decay times and α_i are the pre-exponential factors (amplitudes) of the individual components ($\Sigma\alpha_i = 1$). The contribution of each component to the steady state intensity is given by:

$$f_i = \frac{\alpha_i \tau_i}{\sum_j \alpha_j \tau_j} \quad (2)$$

where the sum in the denominator is over all the decay times and amplitudes. The mean decay time (intensity-weighted average lifetime) is given by:

$$\overline{\tau} = \sum_i f_i \tau_i \quad (3)$$

and the amplitude-weighted lifetime is given by:

$$\langle \tau \rangle = \sum_i \alpha_j \tau_i \quad (4)$$

The transfer rate for a Förster resonance energy transfer (FRET) mechanism is given by [21–23]:

$$k_T = \frac{\mathcal{Q}_D \kappa^2}{\tau_D r^6} \left(\frac{9000\, ln10}{128\pi N n^4} \right) \int_0^\infty F_D\ (\lambda)\, \varepsilon\, (\lambda)\, \lambda^4\, d\lambda \quad (5)$$

Where r is the distance between the acceptor and donor, Q_D is the quantum yield of the donor in the absence of acceptor; τ_D is the lifetime of the donor in the absence of acceptor; n is the refractive index of the medium; N is Avogadro's number; F_D is the normalized fluorescence intensity of the donor (area under the curve normalized to unity); ε(λ)is the extinction coefficient of the acceptor at λ; k^2 is the orientational factor describing the relative orientation of the transition moments of the donor and acceptor in space. The integral in equation (5), referred to as overlap integral J(λ), expresses the extent of spectral overlap between the donor emission and acceptor absorption and is given by:

$$J\,(\lambda) = \frac{\int_0^\infty F_D\ (\lambda)\, \varepsilon\, (\lambda)\, \lambda^4\, d\lambda}{\int_0^\infty F_D\ (\lambda)\ d\lambda} \quad (6)$$

$F_D(\lambda)$ is dimensionless. If the extinction coefficient ε(λ) is expressed in units of $M^{-1}cm^{-1}$ and λ in nanometers, then J(λ) is in units of $M^{-1}cm^{-1}nm$.

R_0, the characteristic Förster distance, is defined by the equation:

$$R_0 = 8.79 \times 10^3 \left[\mathcal{Q}_D\, \kappa^2\, n^{-4} \quad J\,(\lambda) \right]^{1/6} \quad (7)$$

This expression provides R_0 in Å units, and it represents the distance where the energy transfer rate is equal to the sum of all other deactivation rates (radiative and nonradiative). In our estimation of R_0 we assumed that the vacancy center is located close to the ND surface, and we used the refractive index of 1.4 that corresponds to the densely packed proteins.

RESULTS AND DISCUSSION

Suspensions of FITC labeled BSA and FNDs have been prepared in comparable molar concentrations. Measured fluorescence intensity decay for BSA/FITC solution shows 2 lifetime components (1.2 ns and 3.8 ns) with average lifetime of ~3 ns indicating residual self quenching of FITC molecules. Knowing the molecular weight and extinction coefficient of the protein, it is straightforward to calculate the concentration of the protein in solution, but it is not easy to independently estimate concentration of NDs in suspension. Since objective evaluation of ND concentration is very difficult, we confirmed the concentration of NDs by drying the same amount of highly diluted solutions of protein and NDs (~10 ul) on two glass slides and counting the average number of fluorescent spots. We assume that the concentrations were low enough and we did not have significant aggregation of proteins or NDs. We did a few dilutions and obtained consistent numbers. For our studies we were using comparable concentrations of BSA-FITC, NDs, and NDs/BSA-FITC conjugate.

Fig. (1) shows the absorption spectrum of the BSA-FITC solution in PBS buffer in 1 cm cuvette (green) and when adsorbed to fluorescent NDs (dashed red line) as well as FNDs alone (dotted blue line), both in 4 mm path cuvette. It was necessary to use a thinner cuvette due to the high scattering of NDs that artificially increases absorption. Several critical

observations can be made including a very high scattering from FNDs and from FNDs/BSA-FITC in solution. Very high scattering from the ND suspension is not a surprise since diamond material has a very high refractive index (2.32). Large 35 nm particles are expected to have hundreds-fold higher scattering than a solution of smaller size BSA molecules. Interestingly, protein complexed FNDs have even higher scattering, confirming our estimation that a single ND accommodates a significant number (20–50) of protein molecules that enlarge the overall size of the FND particle. The absorption peak of FITC is clearly present, indicting a significant number of FITC molecules per single FND.

Fluorescence of Single FNDs

A low concentration of FNDs was spin coated on the glass slide (Mentzel) and slowly dried. Fig. (2) shows a selected confocal microscopy image of 35 nm FNDs deposited on a cover slip collected with our single molecule system MT 200 (Picoquant). The excitation wavelength was 470 nm and observation was made through a 650 nm long pass cutoff filter. Bright fluorescent spots are clearly visible. The brightness of individual spots is relatively high and varies significantly due to different numbers of fluorescent (N-V) centers in individual diamonds. We also cannot exclude occasional ND aggregation. The selected region shown in Fig. (2) represents a 1.5 micron × 1.5 micron area containing two fluorescent spots (two FNDs). In this Figure we also show the time-dependent intensity trace (B) for a selected single spot. The fluorescence is extremely photostable, and for over 10 min, it does not change or blink. In selected studies, we maintained the light exposure for over 30 min and did not see significant changes. From the collected image in Fig. (2) we obtained time-resolved histogram (intensity decay - C) and calculated fluorescence lifetimes (shown as an insert in Fig. (2B)). Two fluorescence lifetimes are observed, a dominant 13.4 ns component and a small fraction of a 3.3 ns component resulting in an average fluorescence lifetime of 12.6 ns. In Fig. (2D) we present the fluorescence lifetime distribution for the major long lifetime component (13.4 ns).

Fluorescence of Single FND-BSA-FITC Conjugates

Similar to bare FNDs, we spin coated the low concentration suspension of FND-BSA-FITC conjugates on a slide and slowly dried it. We again used the 470 nm excitation and two channels for fluorescence observation. One channel was equipped with a 650LP filter for emission longer than 650 nm and the second channel for fluorescein emission was equipped with a 510 nm band pass filter ±20 nm (510/40BP Semrock). The FITC emission has a maximum at ~520 nm, and it practically ends by 650 nm. The first channel (650 nm long pass) therefore sees FNDs with little if any direct contribution from FITC. We estimate that the long wavelength emission tail of FITC may contribute a maximum 2–3 % of the total signal. We were not able to reliably detect pure BSA-FITC deposited on glass through 650LP channel. The representative image of the emitting spot is shown in Fig. (3). The top two panels show the images of a single FND-protein complex seen by 650LP (left) and 510/40BP (right). The average fluorescence lifetimes are 11.36 ns and 2.03 ns, respectively. Clearly the emission of fluorescein is quenched in labeled BSA molecules when bound to FND. One possible explanation is the presence of FRET. The average fluorescence lifetime in the 650LP channel was 11.36 ns, shorter than in Fig. (2). This was consistent through the number of spots we observed. We are not surprised with this result since this reflects the

minor contribution from FITC emission leaking into 650LP channel. After the initial scan we exposed the selected spot to 10 times higher intensity of light. After 10 min we rescanned the image. The intensity in channel 650LP dropped by almost 50% and the fluorescence lifetime recovered to 12.4 ns, to the value expected for FND only. In the FITC channel (510/40BP) there was no signal. The FITC was clearly photobleached.

In Fig. (4) we present photobleaching traces for both channels (FITC and FNDs). For this experiment, the intensity of excitation was 5 times lower than in the previous experiment shown in Fig. (3). The photobleaching of FITC shows a fast bleaching component (most likely FITC molecules not participating in FRET) and a much more slowly bleaching component. Interestingly the decrease in the intensity of FNDs does not show the fast bleaching component of FITC but reflects a similar pattern as with the slow FITC bleaching component that stabilizes after ~500 s (exactly when FITC bleached out completely). To explain this behavior we have to take into account that BSA is about 4 nm × 7 nm in size. As it sticks to the FND surface, some of the dyes are close to the surface while others can be as far as 70 Å away. A (N-V) center could be located up to 10 Å under the surface. With the estimated R_0 of about 30–35 Å, FITC molecules located at distance greater than 50 Å from the surface will not or only minimally transfer excitation energy to the (N-V) color centers. The distant fraction of FITC that does not transfer will have a longer fluorescence lifetime and will bleach quickly with the kinetic constant similar to free FITC on BSA. Only FITC molecules that are closer than 40 Å will participate in FRET to the FND fluorescent centers. This fraction of FITC molecules will be quenched resulting in shorter fluorescence lifetime for FITC and better photo-stability. We expect that initially we detect the fast bleaching of dyes far from the surface followed by slower bleaching probes participating in FRET as clearly reflected by the FND time-dependent emission trace Fig. (4). To estimate FITC leakage into the 650LP channel we used BSA-FITC only (no FNDs) deposited on a glass slide. For an initial intensity of ~12 counts/ms at the 510/40BP channel, the reading in channel 650LP was below 0.8 count/ms. So, we are confident that the observed changes in Fig. (4) for channel 650LP are NOT due to the contamination (direct leakage) from FITC emission, but due to the FRET pumping of the FND vacancies that emit at longer wavelengths. We need to add that FITC distant from ND surface, when excited, may also donate excitation energy via energy migration to other FITC molecules on BSA [22, 24] that are closer to the ND surface. Such a multistep process for average labeling efficiency of 7 is feasible; however, its contribution to the overall emission of FND centers will be smaller. In our earlier work [24] we did study such an energy migration process on antibodies and observed the energy exchange for just 3 or even 2 labels.

CONCLUSIONS

Our initial studies suggest that FRET can be an efficient process for pumping the FND vacancies by fluorophores close to the ND surface. This opens many possibilities for the rational design of optical probes based on $(N\text{-}V)^-$ defect pairs in FND. In this proof-of-concept work we used a simple approach based on physical adhesion of dye labeled proteins to the FND surface. This is a statistical process that cannot be precisely controlled or tuned. We are now developing a more rational approach for introducing multiple fluorophores on the ND surface based on both direct labeling and the use of scalable, versatile dendrimer

chemistry. Based on this approach we can develop FNDs coated with probes very close to ND surface or dendrimers that vary in chemical composition, thickness, and number and types of auxiliary groups displayed. Using a different order of grown dendrimers we can regulate the number of dyes and their distance from the ND surface. By using different pumping fluorophores we can tune excitation wavelength from blue to over 550 nm. Using multiple fluorophores located close to the surface we can significantly enhance the overall extinction coefficient. Also to increase FRET efficiency it will be desirable to use smaller NDs. Recently Baranov et al. have shown that small 5 nm FNDs can be produced with significant number of fluorescent vacancies [25]. For such much smaller NDs most of the fluorescent vacancies can be very close to the donor located near the surface.

REFERENCES

[1]. Kelloff GJ, Krohn KA, Larson SM, Weissleder R, Mankoff DA, Hoffman JM, Link JM, Guyton KZ, Eckelman WC, Scher HI, O'Shaughnessy J, Cheson BD, Sigman CC, Tatum JL, Mills GQ, Sullivan DC, Woodcock J. The progress and promise of molecular imaging probes in oncologic drug development. Clin. Cancer Res. 2005; 11:7967–7985. [PubMed: 16299226]

[2]. Godavarty A, Eppstein MJ, Zhang C, Theru S, Thompson AB, Gurfinkel M, Sevick-Muraca EM. Fluorescence-enhanced optical imaging in large tissue volumes using a gain-modulated ICCD camera. Phys. Med. Biol. 2003; 48:1701–1720. [PubMed: 12870578]

[3]. Reubi JC. Peptide receptors as molecular targets for cancer diagnosis and therapy. Endocr. Rev. 2003; 24:389–427. [PubMed: 12920149]

[4]. Jaffer FA, Weissleder R. Molecular Imaging in the Clinical Arena. JAMA. 2005; 293:855–862. [PubMed: 15713776]

[5]. Flaumenhaft R, Tanaka E, Graham GJ, De Grand AM, Laurence RG, Hoshino K, Hajjar RJ, Frangioni JV. Localization and quantification of platelet-rich thrombi in large blood vessels with nearinfrared fluorescence imaging. Circulation. 2007; 115:84–93. [PubMed: 17179017]

[6]. Lakowicz, JR. Long lived Metal-ligand complexes. Vol. Chapter 20. Kluwer Academic/Plenum Publisher; 1999. Principles of Fluorescence Spectroscopy; p. 573

[7]. Davies G, Hamer MF. Optical studies of the 1.945 eV vibronic band in diamond. Proc. R. Soc. Lond. A. 1976; 348:285–298.

[8]. Bradac C, Gaebel T, Naidoo N, Sellars ML, Twamley J, Brown LJ, Barnard AS, Plathotnik T, Zvyagin AV, Rabeau JR. Observation and control of nitrogen-vacancy centers in discrete nanodiamonds. Nature Nanotechnol. 2010; 5:345–349. [PubMed: 20383128]

[9]. Chao J-I, Perevedentdeva E, Chung P-H, Liu K-K, Cheng C-Y, Chang C-C, Cheng C-L. Nanometer-sized diamond particle as probe for biolabeling. Biophys. J. 2007; 93:2199–2208. [PubMed: 17513352]

[10]. Fu C-C, Lee H-Y, Chen K, Lim T-S, Wu H-Y, Lin P-K, Wei P-K, Tsao P-H, Chang HC, Fan W. Characterization and application of single fluorescent nanodiamonds as cellular biomarkers. PNAS. 2007; 104:727–734. [PubMed: 17213326]

[11]. Chang Y-R, Lee H-Y, Chen K, Chang C-C, Tsai D-S, Fu C-C, Lim T-S, Tzeng Y-K, Fang C-Y, Han C-C, Chang H-C, Fann W. Mass production and dynamic of imaging of fluorescent nanodiamonds. Nature Nanotechnology. 2008; 3:284–288.

[12]. Ho D. Beyond the Sparkle: The impact of nanodiamonds as biolabeling and therapeutic agents. NANO. 2009; 3(12):3825–3829.

[13]. Smith LM, Sanders JZ, Kaiser RJ, Hughes P, Dodd C, Connell CR, Heiner C, Kent SBH, Hood LE. Fluorescence detection in automated DNA sequence analysis. Nature. 1986; 321:674–679. [PubMed: 3713851]

[14]. Prober JM, Trainor GL, Dam RJ, Hobbs FW, Robertson CW, Zagursky RJ, Cocuzza AJ, Jensen MA, Baumeister K. A system for rapid DNA sequencing with fluorescent chain-terminating dideoxynucleotides. Science. 1987; 238:336–343. [PubMed: 2443975]

[15]. Vlasov II, Shenderova O, Turner S, Lebedev OI, Basov AA, Sildos I, Rahn M, Shirayev AA, Van Tendeloo A. Nitrogen and luminescent nitrogen-vacancy defects in detonation nanodiamond. Small. 2010; 6:687–694. [PubMed: 20108229]

[16]. Tisler J, Balasubramanian G, Naydenov B, Kuselov R, Grotz B, Reuter R, Boudou JP, Curni PA, Sennour M, Thorel A, Borsch M, Aulenbacher K, Erdman R, Hemmer PR, Jelezko F, Wrachtrup J. Fluorescence and spin properties of defects in single digit nanodiamonds. ASC Nano. 2009; 3:1959–1965.

[17]. Dantelle G, Slablab A, Rondin L, Laine F, Carrel F, Bergonzo P, Perruchas S, Gacoin T, Treussart F, Roch JF. Efficient production of NV colour centers in nanodiamonds using high energy electron irradiation. J. Luminescence. 2010; 130:1655–1658.

[18]. Faklaris O, Botsoa a J, Sauvage b T, Roch a J-F, Treussart F. Photoluminescent nanodiamonds: Comparison of the photoluminescence saturation properties of the NV color center and a cyanine dye at the single emitter level, and study of the color center concentration under different preparation conditions. Diamond & Related Materials. 2010; 19:988–995.

[19]. Demas JN, DeGraff BA. Design and applications of highly luminescent transition metal complexes. Anal. Chem. 1991; 63:829–837.

[20]. http://www.picoquant.com/_scientific.htm

[21]. Förster T. Experimentalle und theoretische Untersuchung des zwischenmolekularen. Uebergangs von Elektronenanregungsenergie. Z Naturforsch. 1949; 4A:321–327.

[22]. Gryczynski, Z.; Gryczynski, I.; Lakowicz, JR. Basics of Fluorescence and FRET. Periasami, A.; Day, RN., editors. Oxford Unversity Press; 2005. p. 21-56.

[23]. Shih W, Gryczynski Z, Lakowicz L, Spudich J. A FRET-based sensor reveals ATP hydrolysis dependent large conformational changes and three distinct states of the molecular motor myosin. Cell. 2000; 102:683–694. [PubMed: 11007486]

[24]. Luchowski R, Matveeva EG, Gryczynski I, Terpetschnig EA, Patsenker L, Laczko G, Borejdo J, Gryczynski Z. Single Molecule Studies of Multiple-Fluorophore Labeled Antibodies. Effect of Homo-FRET on the Number of Photons Avaliable Before Photobleaching. Curr. Pharmaceut. Biotechn. 2008; 9:411–420.

[25]. Baranov PG, Soltamova AA, Tolmachev DO, Romanov NG, Babunts RA, Shakhov FM, Kidalov SV, Vul AY, Mamin GV, Orlinskii SB, Silkin NI. Enormously High Concentrations of Fluorescent Nitrogen-Vacancy Centers Fabricated by Sintering of Detonation Nanodiamonds. Small. 2011; 7(11):1533–1537. [PubMed: 21520495]

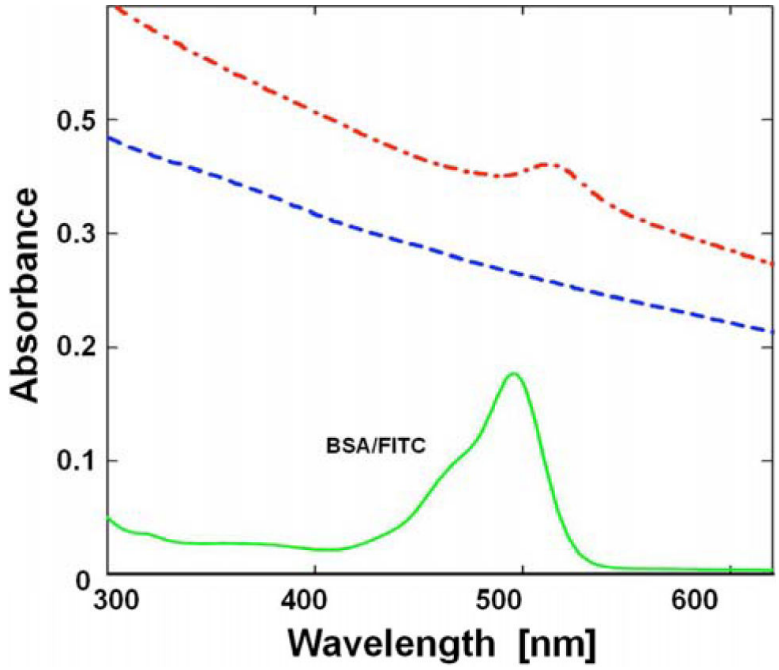

Fig. (1).

Absorption spectra of BSA labeled with FITC (solid); FNDs only (dashed); FNDs labeled with BSA-FITC (dash/dot); and the absorption spectrum of BSA-FITC after subtraction of scattering (solid).

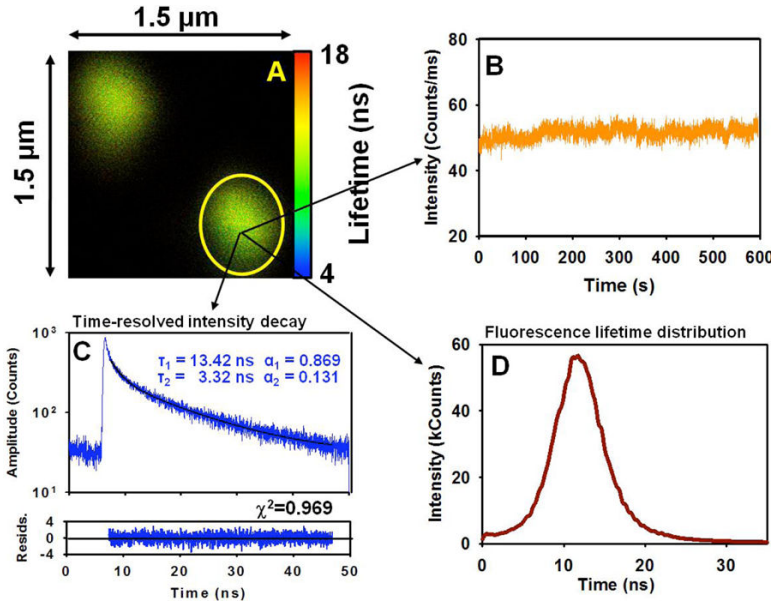

Fig. (2).

A) Image of a small area 1.5 µm × 1.5 µm of FNDs deposited on the glass slide. **B**) Photostability trace. **C**) Time-resolved intensity decay. **D**) Fluorescence lifetimes distribution in the marked area.

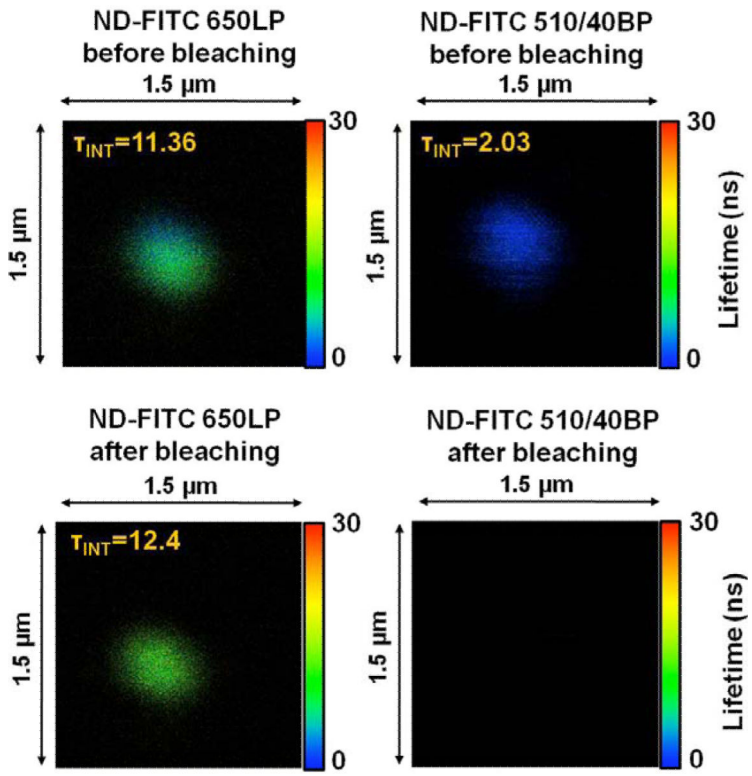

Fig. (3).

Fluorescence image of 35 nm FND labeled with BSA-FITC. Fluorescence signal was observed in two channels. Left 650 nm long pass (650LP) and right 510 nm (40 nm band pass) – Fluorescein channel. Upper panels before light exposure and bottom after light expose.

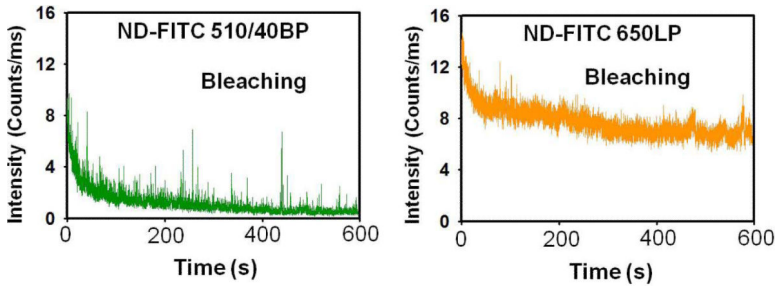

Fig. (4).
Phtobleaching traces simultaneously observed in two channels FITC (left) and FNDs (right).